


FULL PAPER

Open Access



Laser link experiment with the Hayabusa2 laser altimeter for in-flight alignment measurement

Hiroto Noda^{1*} , Hiroo Kunimori², Takahide Mizuno³, Hiroki Senshu⁴, Naoko Ogawa⁵, Hiroshi Takeuchi³, Chris Moore⁶, Alex Pollard⁶, Tomohiro Yamaguchi⁵, Noriyuki Namiki¹, Teiji Kase⁷, Takanao Saiki⁵ and Yuichi Tsuda⁵

Abstract

We report results of a laser link experiment between a laser altimeter called light detection and ranging (LIDAR) aboard Hayabusa2 and ground-based satellite laser ranging stations conducted when the spacecraft was near the Earth before and after the gravity assist operation. Uplink laser pulses from a ground station were successfully detected at a distance of 6.6 million km, and the field of view direction of the receiving telescope of the LIDAR was determined in the spacecraft frame. The intensities of the received signals were measured, and the link budget from the ground to the LIDAR was confirmed. By detecting two successive pulses, the pulse intervals from the ground-based station were transferred to the LIDAR, and the clock frequency offset was thus successfully calibrated based on the pulse intervals. The laser link experiment, which includes alignment measurement of the telescopes, has proven to be an excellent method to confirm the performance of laser altimeters before they arrive at their target bodies, especially for deep space missions.

Keywords: Hayabusa2, LIDAR, Laser altimeter, Laser link, SLR

Introduction

In recent years, laser altimeters have been installed on lunar and planetary exploration missions (e.g., Clementine, NEAR, Mars Global Surveyor, Hayabusa, MESSENGER, Kaguya, Chang'E-1, Chandrayaan-1, and the Lunar Reconnaissance Orbiter) and have contributed significantly to the measurement of planetary topography. Laser altimeters also play an important role in spacecraft navigation as bus instruments. For example, in the Hayabusa asteroid sample return mission, a laser altimeter was used for autonomous navigation by determining the spacecraft's absolute position with respect to the asteroid during the touchdown sequence. Almost all laser altimeters aboard planetary missions consist of a transmitting

telescope, which emits laser pulses, and a receiving telescope, which detects the photons reflected from the surface of the planet. The boresight of both telescopes must be co-aligned to enable detection of laser footprints on the surface of the planet by the receiving telescope. The direction of the fields of view of telescopes in the spacecraft frame (here called the FOV axes) is also important for retrieving the planetary topography data because the telescope pointing direction is determined using spacecraft attitude data. During integration testing before a launch, alignment is established using alignment mirrors. However, it is possible that this alignment may be compromised by the shock of the launch and subsequent thermal environment changes after the launch. Therefore, in situ measurements of alignment are essential. It may be possible to estimate alignment using prominent surface features such as boulders by comparing altimeter data to images taken with cameras, the FOV axes of which are typically well-determined based on calibration with images of stars or planets.

*Correspondence: hirotomo.noda@nao.ac.jp

¹ National Astronomical Observatory of Japan, Mitaka, Tokyo 181-8588, Japan

Full list of author information is available at the end of the article

However, surface features on asteroids are difficult to recognize from ground-based observations, and it is often unclear whether such prominent features really exist. Therefore, other means of estimating the FOV axes are highly desirable. For example, the laser altimeter on Hayabusa was used to determine the FOV axes by detecting the footprints of laser shot with the Near-Infrared Spectrometer (NIRS) during the exposure time because it was sensitive to the 1 μm wavelength of the laser altimeter (Abe et al. 2006). Laser link experiments between ground-based satellite laser ranging (SLR) stations and laser altimeters may also provide an alternative method. Such experiments have been conducted at lunar distance by the Lunar Reconnaissance Orbiter (LRO) (Sun et al. 2014), at 23 million km by the MESSENGER spacecraft (Smith et al. 2006), and at 80 million km by the Mars Global Surveyor (Abshire et al. 2006).

Laser link experiments may be useful not only for alignment measurement but also for performance checks, demonstrations of optical communications, and time transfer to spacecraft from well-calibrated clocks on the ground. Notably, time transfer has recently become an active area of research in the SLR community. This field was first studied by a French research group in the 1980s; the first experiments were undertaken using the laser synchronization from a stationary orbit (LASSO) instrument aboard MeteoSat-P2 in 1992 (Fridelance and Veillet 1995). Since those early experiments, global navigation satellite system (GNSS) experiments have been conducted using a Compass satellite (Yang et al. 2008), and an experiment called time transfer by laser link (T2L2) onboard the JASON-2 spacecraft launched in 2008 was very successful; many ground stations participated in the time transfer experiment (Samain et al. 2010). These experiments are used to compare clocks not only between ground stations and spacecraft but also between different ground stations via spacecraft. Such comparisons can be used to reduce errors of various parameters used in precise orbit determination, including precise estimation of atmospheric delay (Prochazka et al. 2011). Typically, once a two-way link is established between a ground station and the laser reflector onboard the spacecraft, an onboard photon detector is used to time-tag detected laser pulses from the ground, which allows the satellite clock to be calibrated against the clock on the ground (Fridelance et al. 1997).

The Hayabusa2 spacecraft was launched on December 3, 2014, as the second Japanese explorer to the asteroid 162173 Ryugu. It is equipped with a laser altimeter called light detection and ranging (LIDAR) for navigation, scientific observations (Mizuno et al. 2016), and laser link experiments. Such experiments were conducted, while

the spacecraft was near the Earth before and after the gravity assist operation.

A transponder mode was added to the LIDAR system so that it would wait for a laser pulse from the ground station that, once detected, would trigger transmission of a new laser pulse back in the same direction; two-way laser ranging can thus be carried out at planetary distances. In addition, this mode allows two laser pulses to be detected within a given waiting period such that measurements of the time intervals between the two pulses can be returned to the ground as telemetry data via the standard microwave link. This allows the known pulse interval on the ground to be used to calibrate the onboard clock.

The purposes of this laser link experiment can be summarized as follows:

1. Estimating the LIDAR FOV axis and checking the alignment between the transmitting and receiving telescopes if a two-way laser link is established.
2. In-flight testing of the laser link budget.
3. Synchronous two-way ranging at planetary distances, i.e., farther than the lunar distance, as a technological demonstration.
4. Testing the new time transfer technique for onboard clock calibration as a technological demonstration.

Next, we describe the alignment requirement from the perspective of asteroid remote sensing.

Asteroids are a category of solar system objects that are considered the remains of the building blocks of planets in the solar system. Porosity is a key parameter for asteroids; this parameter can be used to determine whether an asteroid is monolithic or rubble-pile after a long history of collision and aggregation. It is therefore a major factor in controlling asteroid evolution. Global porosity can be estimated from mean density which is calculated from the volume and mass, and density of the rocks that form the asteroid. In the case of Hayabusa2, optical images taken with a camera are scaled by the LIDAR range data, and these images are used to create a global shape model. Range data to the asteroid during free-fall toward it are used to estimate its total mass and the regional gravity field. Rock types can be estimated based on remote sensing data from instruments such as optical and infrared spectrometers and from samples to be returned in 2020. All of these data are combined to estimate porosity. If the porosity can be estimated with error <10%, the asteroid can be identified as monolithic or fractured. This error corresponds to 5% error in volume estimation or the shape model, which is the required level of accuracy for asteroid science (Namiki et al. 2014).

Here, we estimate the impact of uncertainty in determining the FOV axis. If the angular uncertainty of its direction is $\Delta\theta$, the distance to the asteroid is D , and the surface slope is α , the error of the LIDAR range associated with the shift in the laser footprint position from the position without uncertainty is approximately $D(\Delta\theta) \sin \alpha$. For example, if a ranging measurement of a position with a 30° slope is made from the location called the “home position,” with a distance of about 20 km from the target asteroid (162173 Ryugu), the error of the range will be $10 * \Delta\theta$ (m), with $\Delta\theta$ given in milliradians. Therefore, even 1 mrad of uncertainty can influence the interpretation of local topography.

The structure of this paper is as follows. Section two describes the hardware and the experimental setup. The results of the experiment are presented in section three, followed by discussion in section four and a summary in section five.

Experimental methods

This laser link experiment consists of the ground segment and flight segment. A ground-based telescope emits and receives laser pulses. The flight segment includes the spacecraft system and the laser altimeter. We call the link from the ground-based station to the spacecraft the “uplink” and that from the spacecraft to the ground the “downlink.” A ground station in either Japan or Australia transmits the uplink laser, and the LIDAR receives the laser and transmits the laser downlink when the LIDAR is in the laser link mode. In range mode, both the ground-based station and the LIDAR transmit and receive laser pulses independently. A description of each segment is provided in the following sections, followed by an analysis of the associated link budget.

Flight segment

LIDAR hardware and observational modes

The LIDAR aboard Hayabusa2 is an instrument for ranging that uses Cr, Nd:YAG laser pulses with a wavelength of 1064 nm. In addition to the basic function of the LIDAR aboard the Hayabusa spacecraft (Mizuno et al. 2006), several improvements have been implemented, including:

1. The addition of the ability to monitor transmitting pulse intensity.
2. The application of a passive Q-switch to resolve a problem with laser pulse emission associated with malfunctioning of the active Q-switch.
3. The addition of the transponder mode and dust counting mode (Senshu et al. 2016).

The basic parameters of the Hayabusa2 LIDAR are shown in Table 1. For detailed specifications, see Mizuno

Table 1 Specifications of the LIDAR

Item	Value
Measurement range	30 m→25 km
Range resolution	0.5 m
Laser	
Wavelength	1064 nm
Energy	15 mJ
Pulse width	7 ns
Beam divergence	2.4 mrad, full angle
Repetition rate	1 Hz Max., externally triggered
Receiver	
Long range (>1 km)	Diameter 110 mm, FOV 1.5 mrad
Short range (<1 km)	Diameter 3 mm, FOV 20.4 mrad
Detector	Si-APD-HIC, bandwidth 100 MHz

et al. (2016). The LIDAR is triggered with 1 pps signals delivered from the spacecraft, and the maximum repetition rate of the laser is 1 Hz. Yamada et al. (2016) evaluated the performance of the detector in an experiment in which constant laser pulses were introduced into the receiving telescope and the output signal levels were measured. Estimated deviation of the receiving power of the laser at the detector was about 5%.

Mainly, for this experiment, the transponder mode was used. In this mode, a link start command configures the instrument to wait for a maximum of 1 s for a laser pulse from the ground. If a signal that exceeds the threshold level is detected by the receiving telescope, the signal will trigger laser emission of 15 mJ. Two laser pulses can be detected during the 1-s waiting period, which provide pulse interval measurements. After a command is given to fetch data from the LIDAR, these measurements are sent to the ground via microwave link. As a result, it takes 2 s to acquire one set of data. To determine whether uplink pulses were detected, it was necessary to use first and second detection flags because receiving intensity data were not available. The LIDAR must be in range mode to determine the detection level. Further explanation of the observational modes is given in “[Appendix 1: Observational modes of LIDAR](#)”.

The following is a summary of the parameter settings of the LIDAR. Thresholds of 14.4 mV were set during the spacecraft’s scanning in transponder mode and during fixed spacecraft pointing, 46.1 mV during transponder mode, and 27.1 mV during range mode. The APD gain multiplier M was generally set to high ($M = 100$, responsivity = 500 kV/W, parameter setting = 8). During reduced gain tests, the APD gain multiplier was set to low ($M = 10$, responsivity = 50 kV/W, parameter setting = 2).

Spacecraft operations and timing

Initially, the experimental periods were determined based on spacecraft attitude constraints before and after the gravity assist operation. During the experiment, two conditions had to be met: the +Z plane of the spacecraft had to face the Sun for power generation, and the -Z plane had to point toward the Earth. In other words, the spacecraft needed to be operated safely for the gravity assist operation, and the LIDAR FOV axis needed to be pointed toward the Earth while enough electrical power was available.

The second condition can be met if the Sun-Probe-Earth (SPE) phase angle is greater than 120°; this requirement was used to identify and assign 4 days in both October and November 2015, and 8 days in December 2015, for the experiment. The SPE angles and the distances between the spacecraft and the Earth during these periods are shown in Fig. 1, and the relative position between the Earth and spacecraft is shown in Fig. 2.

Spacecraft scan constraints

To determine the direction of the LIDAR FOV axis, the spacecraft was scanned with small angles while a ground station fired laser pulses. The scan was carried out using the reaction wheels of the spacecraft, while the attitude of the spacecraft was detected with the star tracker. Attitude determination was accurate to 0.03° (0.5 mrad). The settling time for a small-angle attitude maneuver is typically about 30 s. However, the experimental data are valid even if the attitude of the spacecraft had not yet reached its final stable position. Therefore, to reduce the operation time, data acquisition was initiated before attitudes were stable. A spiral scan was adopted with a central

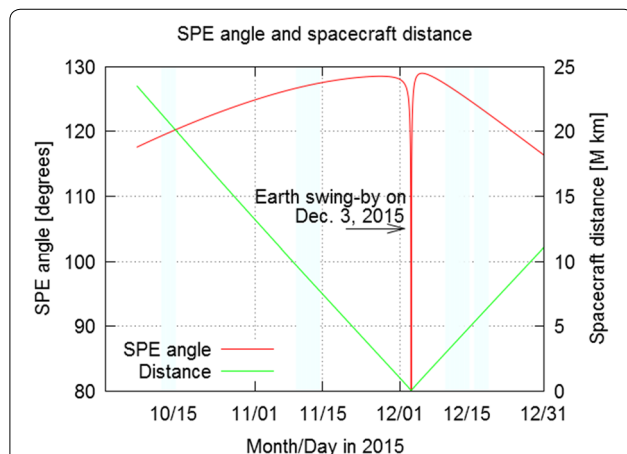


Fig. 1 Time-series of SPE angle and spacecraft distance from the Earth. SPE angles in degrees and distances in million km (10^6 m) are shown on the left and right vertical axes, respectively. Dates of experiments are indicated with light blue boxes

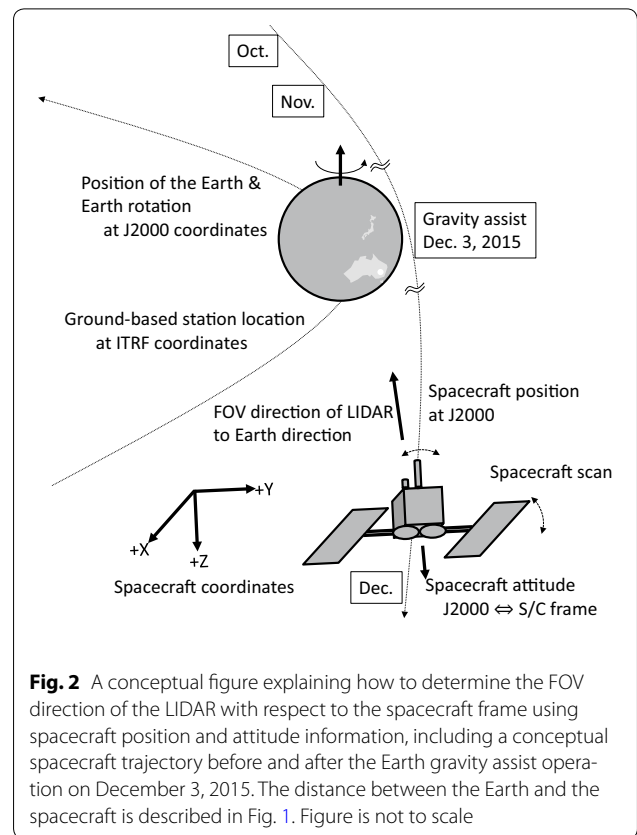


Fig. 2 A conceptual figure explaining how to determine the FOV direction of the LIDAR with respect to the spacecraft frame using spacecraft position and attitude information, including a conceptual spacecraft trajectory before and after the Earth gravity assist operation on December 3, 2015. The distance between the Earth and the spacecraft is described in Fig. 1. Figure is not to scale

direction considered the boresight of the LIDAR from the pre-flight alignment test. The scan step was 1 mrad, which is slightly smaller than the 1.5 mrad FOV of the receiving telescope.

The duration of the LIDAR operation was determined based on several factors. When the spacecraft was not visible from the Earth, the limiting factor was the total number of commands available for the LIDAR, and when the spacecraft was visible, the limiting factors were the allocated time for operation of the LIDAR within the daily operation and the duration of the laser shot at the ground-based station. As a result, the duration was determined as 2 h for visible periods, and 1 h for non-visible periods from the Earth. It was planned that the scan would cover a square area of $1^\circ \times 1^\circ$ over 4 days, which was considered the area over which the field of view direction would surely be found. Finally, the time period for an attitude of the spacecraft was set as 40 s, which included 17 sets of 2-s continuous link start and status request commands, such that 17 data points could be acquired in 34 s. The total number of scans per hour was 92.

The orbit prediction files for each day were created from precise orbit determination results based on one-week range and range rate observations by microwave

link. In addition, an observed-minus-calculated ($O - C$) value of the range in the line of sight to the spacecraft was estimated an hour before each LIDAR experiment using <30-min microwave ranging; the $O - C$ value could therefore be used to set the range gate of the ground-based laser detection system. The typical $O - C$ values were 100–300 m (0.3–1 μ s) in the line of sight direction, depending on the age of the precise orbit determinations.

Timing system

The Hayabusa2 time system is based on an onboard clock called the Time Index (TI), the minimum unit of which is approximately 31.25 (=1000/32) ms. However, actual values vary slightly from 31.25 ms because of temperature drift of the crystal oscillator. The TI and Coordinated Universal Time (UTC) are compared on a regular basis based on downlinked packets that include onboard TIs and the receiving times of each packet on the ground. The length of the TI at each moment is then derived by interpolating the TI–UTC observations. Note that the duration of the 1 pps signal that triggers the LIDAR measurement is generated as 32 TIs; therefore, the 1 pps intervals drift by a small amount with respect to UTC seconds.

Ground segment

The orbit of the spacecraft near the time of the Earth gravity assist operation on December 3, 2015 was such that the spacecraft approached the Earth from the north, and its trajectory after the gravity assist was southward, as shown in Fig. 2. Therefore, ground station laser tracking was planned for Japan in October, for both Japan and Australia in November, and for Australia in December. Because the footprints on the Earth from the spacecraft would be sunlit (afternoon to evening on the Earth) in October and November, it was expected that the background noise would be greater than non-sunlit periods. As a result, it was planned that the October and November experiments would be dedicated to the search for the LIDAR FOV axis direction by detecting the laser from the ground and that the downlink experiment would only be possible during the Earth’s nighttime in December.

Most SLR stations use green lasers with wavelengths of 532 nm; relatively few SLR ground stations are equipped for laser transmission at 1064 nm, which is the wavelength required for the LIDAR system. The Mt. Stromlo observatory in Canberra, Australia is one of very few stations that can emit and receive at 1064 nm. The National Institute of Information and Communications Technology (NICT) Koganei station in Tokyo was prepared with a 1064 nm laser system for this experiment. Therefore, these two ground stations were selected to provide ground-based observations. The specification of both ground stations are listed in Table 2.

Table 2 Specifications of the ground stations

	Koganei	Mt. Stromlo
Laser		
Wavelength (nm)	1064	1064
Energy (J)	1	2.2
Pulse width (ns)	10	15
Beam divergence (full angle) (arcsec)	20 ± 2	12 ± 2
Repetition rate (Hz)	10	170
Receiver		
Diameter (m)	1.5	1.8
Field of view (full angle) (arcsec)	45	20
Detector	InGaAs APD-array	IR-enhanced Si-APD

The time standard of the Mt. Stromlo station is a Symmetricom XLi GPS clock with a frequency generated by a temperature compensated crystal oscillator (TCXO). The Allan variance for 1 s of this time standard is about 1 ns. The repetition rate is 170 Hz. However, because the time resolution of the laser timing system is 100 ns, it was apparent that the time intervals between two pulses used for the time transfer experiment had a jitter of 100 ns in addition to 1/170 Hz (5.882 ms). A more detailed description of the Mt. Stromlo observatory is given by Smith et al. (2012).

Laser link budget

In this subsection, we describe the laser link budget. The laser energy, the diameter of the receiving telescope and the responsivity of the LIDAR are designed such that ranging is possible from a position 25 km from the surface of the asteroid with an albedo of 6% (Mizuno et al. 2016). A possible link from the ground-based SLR station was assessed through a simple calculation. The receiving power as output voltage of the APD can be estimated using:

$$V = P_t \eta_t \times \frac{\pi r^2 \eta_r}{D^2 \cdot \pi \theta_t^2} \times L_0 \times R_{APD},$$

where the laser power from the ground is P_t (W), the efficiency of the transmitting telescope is η_t , the beam divergence of the transmitting laser (half cone) is θ_t (rad), the distance from the ground to the spacecraft is D (m), the radius of the receiving telescope is r (m), the total transparency of the receiving telescope (before the entrance of the APD) is η_r , the total efficiency including atmospheric effects and pointing loss is L_0 , and the responsivity of the APD (receiving power—output voltage conversion efficiency) is R_{APD} . Parameter values for

the Australian ground station and LIDAR give $P_t = 2.2$ (J)/15 (ns) = 1.46×10^8 (W), $\eta_t = 0.8$, $\theta_t = 6$ (arc-sec) = 2.9089×10^{-5} (rad), $r = 5 \times 10^{-2}$ (m), $\eta_r = 0.8$, and $R_{\text{APD}} = 500$ kV/W, which allow estimation of V as a function of efficiency, L_0 , and distance, D (million km). Substituting $D = 10$ (million km) as the distance during experiments in November with the Australian station and an efficiency of $L_0 = 0.1$ as a conservative value yields $V = 138$ (mV). Normally, the APD detector generates thermal noise; therefore, a threshold is set for signal detection. In normal observations near the target asteroid of Hayabusa2, a value lower than 30 mV (nominal 27 mV) is set, which corresponds to a power of 6×10^{-8} (W) at a distance of 30 km. Therefore, the above calculations indicate that the LIDAR is capable of detecting laser pulses from the Earth.

For detection of the downlink signal from the spacecraft, the same calculation can be applied by taking into account divergence of the laser pulses. Note that single photon counting is used for detection at the ground-based station; therefore, the number of photoelectrons N is expressed as follows:

$$N = q \times \frac{E\eta_t}{hc/\lambda} \times \frac{\pi r^2 \eta_r}{D^2 \cdot \pi \theta_t^2} \times L_0,$$

where the transmitting energy of the LIDAR is E (J), the transmittance efficiency is η_t , the beam divergence is θ_t (rad), the quantum efficiency of the detector on the ground is q , Planck's constant is h (Js), the laser wavelength is λ (Hz), the speed of light is c (m/s), the radius of the receiving telescope is r (m), the receiving efficiency is η_r , and the total efficiency due to loss is L_0 . By substituting the parameters of the LIDAR and the same values for the Australian ground station, $E = 0.015$ (J), $\eta_t = 0.8$, $\theta_t = 1.25 \times 10^{-3}$ (rad), $r = 0.9$ (m), $\eta_r = 0.8$, and $q = 0.2$, we obtain N as a function of efficiency, L_0 , and distance, D (million km) By substituting $D = 7$ (million km) as a typical distance during experiments in December and a total efficiency of $L_0 = 0.1$, the number of photoelectron is found to be 10.8. Single photon counting is possible; however, detectability is highly dependent on the level of noise.

Results

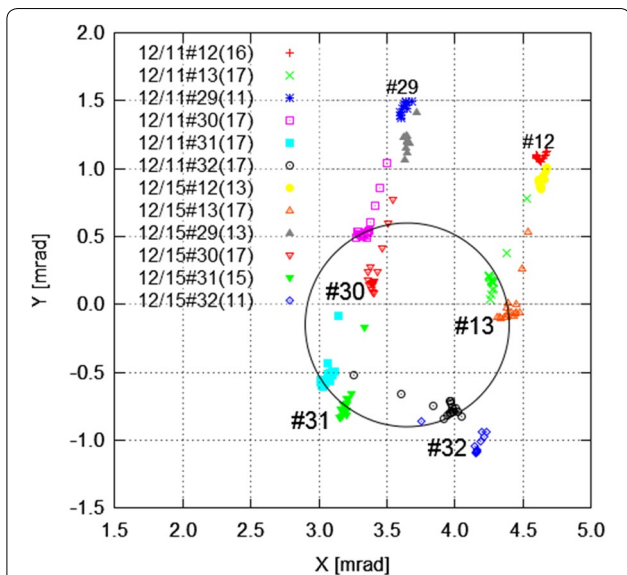
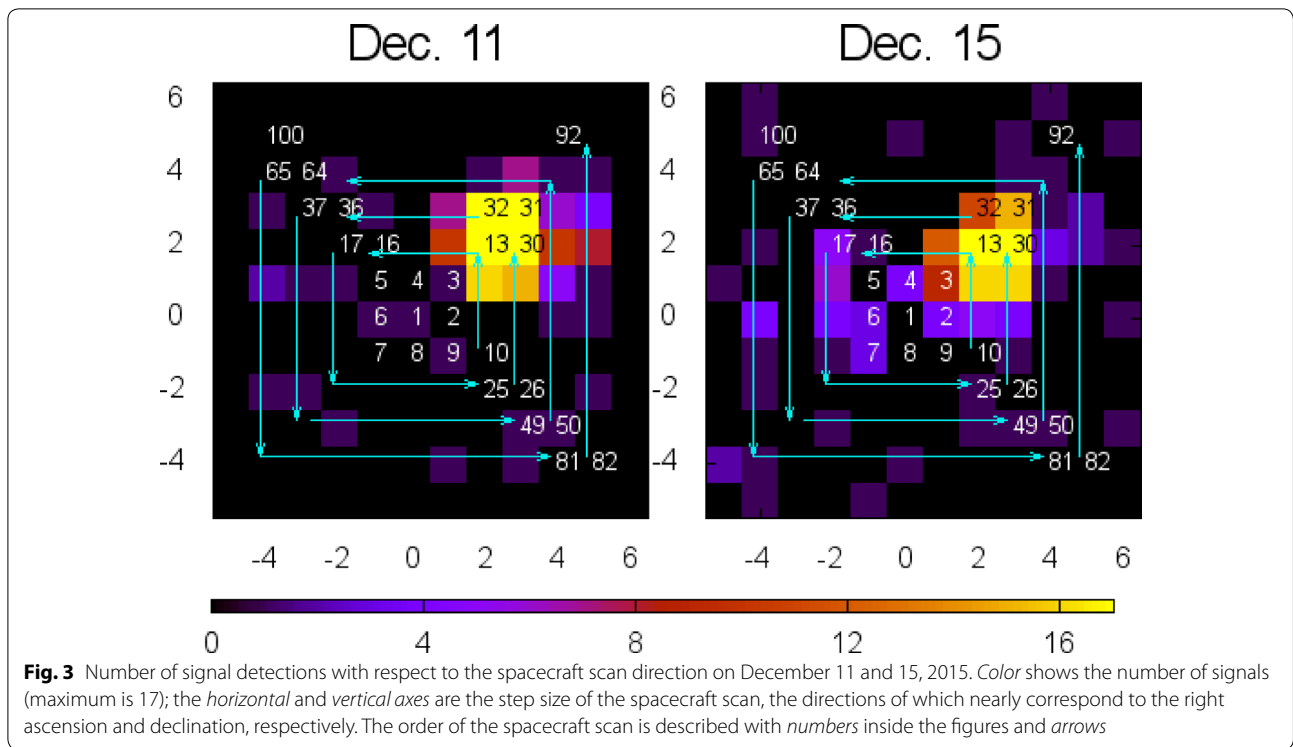
These experiments were carried out for a total of 16 days: October 13–15, November 10–14, and December 11–15 and 17–19. In October and November, no data were obtained because thick clouds blocked the laser transmissions, and the spacecraft scanning schedule could not be changed to avoid these cloudy conditions. Fortunately, favorable weather conditions enabled experiments to be conducted in December.

The scanning operations of the spacecraft were carried out until Dec. 18; it was 1 day before the end of the experiment when we successfully confirmed the boresight direction of the LIDAR telescope. On the final day of the experiment, December 19, fixed pointing of the spacecraft toward the Earth, the small-angle pointing shift of the ground telescope, and the change in the gain of the LIDAR were successfully achieved. As a result, we confirmed that the laser pulses from the ground were detected with the LIDAR. We have not found any evidence that the ground-based station detected return pulses from the LIDAR; consequently, we could not obtain two-way ranges.

Estimation of the LIDAR boresight

We estimated the boresight of the receiving telescope of the LIDAR using the scanning data obtained on December 11 and 15 with the spacecraft scanning method described in section “[Spacecraft scan constraints](#).” Figure 3 illustrates the spacecraft scans as two dimensional tiles. One attitude of the spacecraft scan is presented per tile. The separation angle between each tile is 1 mrad. The horizontal and vertical axes are the step sizes of the spacecraft scan, the directions of which nearly correspond to the right ascension and declination of the pointing direction, and the origin is the best-estimated direction of the boresight obtained during the ground-based prelaunch test. The color in each tile indicates the number of signal detections, and numbers and arrows in the figure represent the order of the spacecraft scans. Purple tiles indicate non-zero detection, which we consider to represent false detections caused by noise. The low threshold level of detection, at 14.4 mV, was significantly lower than the nominal value of 27 mV set for the experiment. As mentioned in section “[Spacecraft scan constraints](#)”, the maximum detection number for one tile is 17 because the LIDAR signal waiting period is 17 s in total. We selected data from when both the first and second pulse flags were detected. A maximum number of 17 was recorded in four tiles (numbers 13, 30, 31, and 32) on December 11 and in two tiles (numbers 13 and 30) on December 15, which allowed determination of the field of view direction of the LIDAR. The direction of the ground station from the spacecraft at each point in time was determined in the J2000 inertial coordinate system using spacecraft orbit data and the position and rotational phase of the Earth. Using spacecraft attitude data, ground station directions were then converted from J2000 to the spacecraft frame, as illustrated in Fig. 2.

Figure 4 shows the directions of the LIDAR FOV on December 11 and 15 projected onto the XY plane of the spacecraft frame as stated above. Note that the units of the X and Y axes in the figure are milliradians because the



direction of the field of view of the LIDAR was close to the $-Z$ direction and that the X and Y components in the spacecraft frame were small. Bracketed numbers in the

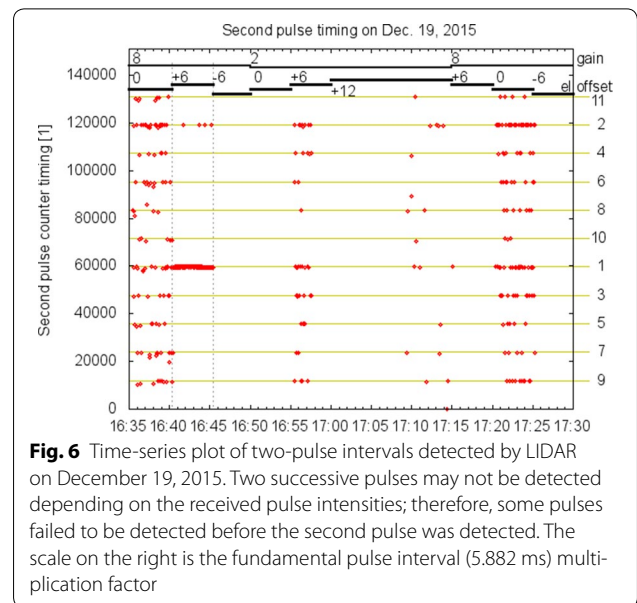
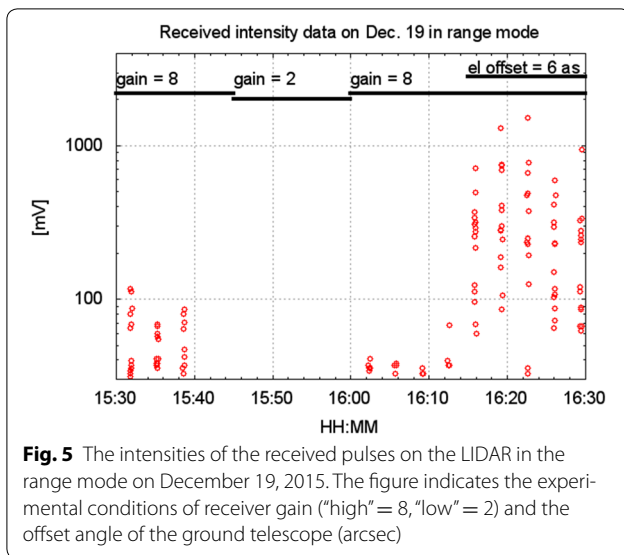
legend indicate how many pulses were detected at a given spacecraft attitude position, up to a maximum of 17. This figure also shows that the estimated total field of view area of the receiving telescope exceeds 1.5 mrad, which was the estimated value before launch.

Based on the above information, we were able to determine the boresight direction of the receiving telescope. Here, we simply determine the center of 1.5 mrad circle that covers the attitude directions of all 17 data recorded on December 11 and 15. Accordingly, the best estimate of the boresight vector was determined to be $(X, Y, Z) = (0.003650, -0.000150, -0.999993)$.

Roughly, the angular separation of the boresight from the $-Z$ axis was 3.5 mrad (0.2°). However, there were other directions in which data were obtained that suggested that the vector may have an error of about 1 mrad (due to the scanning step size).

Intensity of received pulses in range mode

On the last day of the experiments (December 19), we set the LIDAR to range mode for half of the allocated time and tried to measure the reception level of the laser pulses from the ground. The spacecraft attitude was fixed to the ground station direction for this period. The resulting detection levels are shown in Fig. 5. The vertical axis is shown as a logarithmic scale because the received intensity values range from 30 to 1500 mV. The horizontal axis is UTC time (hour/minute). Data in range mode



are sparse because of slight differences between the Time Index (TI) and UTC, as well as the motion of the spacecraft. Detailed information is provided in “Appendix 2: Explanation of sparse data in the range mode”. The gain of the receiver was set as “low” from 15:45 to 16:00 for comparison with other periods of time, and it was found that the signals were not detected with “low” gain. This result was considered reasonable because previous reception levels were between 30 and 100 mV, “low” gain has efficiency 10% of that of “high” gain, and the threshold level was set to 14.4 mV.

After 16:00, the gain was reset to “high”, and between 16:15 and 16:30, the ground station pointing was slightly changed to determine whether the current pointing was correct. The amount of pointing shift was 6 arcsec, which roughly corresponds to half the width of the field of view of the ground telescope. During this period, the received intensity increased by almost tenfold relative to the other periods. Based on this evidence, we confirmed that the signals came from the ground-based laser, not from other sources such as Earth background radiation, because the intensity varied in accordance with the pointing shift.

Intervals between two received pulses

As stated in section “LIDAR hardware and observational modes”, two successive pulses can be detected in the transponder mode during the 1-s waiting time, and the interval between the two pulses is sent as telemetry data. Figure 6 shows a time-series plot of raw telemetry data (STOP2 TIMING telemetry) of pulse intervals from 16:35 to 17:30 on December 19. The vertical axis is the counter value of STOP2 TIMING. Data regarded as noise were removed from this plot.

Most of the data are aligned with eleven lines, which are predicted counter values of the integral multiples (from 1 to 11, shown in the right) of the fundamental pulse interval of 5.882 ms. These values are the remainders of when the total counter values were divided by one counter cycle of 2^{17} . For example, the numbers 1 and 2 indicate that two detected pulses have intervals of 5.882 and 11.764 ms, respectively. Numbers in the upper part of the figure represent the detector gains (2 = low, 8 = high) and the elevation offset angle of the ground telescope. Notably, from 16:40 to 16:45, when the elevation offset angle of 6 arcsec was introduced to the ground telescope, almost all data are clustered at the line segment “1”, which indicates that most of the second pulses were detected immediately after detection of the corresponding first pulses.

It is assumed that this situation was similar to that of the time period 16:15–16:30 when the same offset angle was set during the range mode test sequence. In other time slots, the number of second pulse detections decreased as the integral multiple factor increased (fewer data points for longer pulse intervals). However, from 17:15 to 17:20, although the offset angle was set to the same value, no signal was detected. Instead, the second pulses were detected with an offset angle of zero immediately after this time period.

It is apparent that data points from 16:40–16:45, which almost fall into the “1” category, are divided into two groups with a time difference of about 100 ns. To send ground-based time data to the spacecraft, we must associate each ground pulse with the corresponding pulse detected by the spacecraft. However, identification of

ground pulses at the LIDAR was unsuccessful, mainly because the execution time of the “link start” command at the LIDAR had an ambiguity of more than 1 TI (31.25 ms), while the ground station laser fire rate was 170 Hz (5.882 ms). Therefore, as an alternative method, we compared the histogram of ground pulse intervals and those detected with the LIDAR. These histograms are shown in Fig. 7, where the horizontal axis represents pulse intervals (μs) and the left and right tick marks on the vertical axis indicate frequencies for the ground-based station and the LIDAR, respectively.

The histogram of the ground pulse intervals is expressed as a stair-step plot, whereas that of the LIDAR is shown as bars. The LIDAR intervals were calculated as follows. The cycle ambiguity was added to the raw count data (STOP2 TIMING) of the LIDAR; then, 26 counts were subtracted to correct for spacecraft motion in the line of sight direction over a single interval (4.42 km/s multiplied by 5.882 ms). Here, we used a constant value of 26 counts because the spacecraft was far from the Earth and the observation time was short, and the change in spacecraft velocity was negligible. The counter values were then converted to time using the LIDAR counter clock frequency, and adjusted by 1.874 kHz so that the LIDAR histogram could be overlain on the ground histogram.

Two groups of ground pulse intervals are apparent in the figure. These groups result from the 100-ns time resolution of the ground laser pulse interval, as stated in section “Ground segment”. In addition, it is apparent that the LIDAR pulse intervals also display two groups of data, which differ by 100 ns; each group has a width of several tens of ns. Therefore, we conclude that the ground

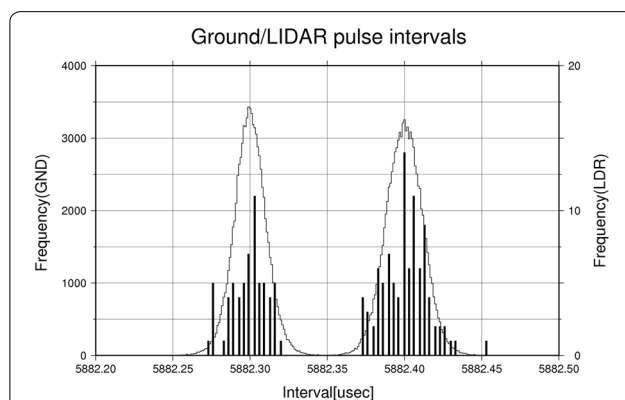


Fig. 7 Histogram of the ground pulse intervals shown as a stair-step plot. The histogram of the LIDAR’s two-pulse intervals is shown as a bar histogram. The clock frequency of the LIDAR counter is adjusted by about 2 kHz from the nominal frequency so that the two histograms overlap. The left and right vertical frequency tick marks refer to the ground station and the LIDAR respectively

pulse intervals match the LIDAR intervals. In addition, the clock frequency of the LIDAR was successfully adjusted by making two histograms overlap. The amount of adjustment was 6 ppm for the 300 MHz counter, which is a reasonable value for normal crystal oscillators. Note that the thermal environment of the spacecraft on this day was generally stable over the 2-h observation period.

Discussion

Boresight of the receiving telescope with respect to the spacecraft frame

The boresight direction of the receiving telescope was determined to have shifted by 0.2° (3.5 mrad) from the best-estimated direction prior to launch (the central position of the spiral scan in Fig. 3). At the same time, the shift from the $-Z$ direction of the spacecraft was also 0.2° .

Originally, the requirements of the LIDAR boresight direction as a navigation tool allowed relative alignment between the Near-Infrared Spectrometer (NIRS3) and LIDAR to be $<1^\circ$, and for the shift from the $-Z$ axis to be $<0.5^\circ$. Therefore, the tolerance of the shift of the telescope with respect to the spacecraft associated with the launch was not defined quantitatively. In addition, the boresight direction before launch was determined based on the measured differences between the LIDAR boresight and an alignment cube on the LIDAR, and between the alignment cubes on the LIDAR and spacecraft. Therefore, the determined prelaunch boresight direction was treated as a reference value, based on the accuracy requirements stated above. It is concluded that a more precise boresight direction with respect to the spacecraft as a scientific instrument was identified in this experiment.

We could not obtain information on the alignment between the transmitting and receiving telescopes. However, a vibration test before launch confirmed that the shift between the two telescopes due to vibration is <0.1 mrad. In addition, according to the thermal vacuum test performed before launch, it is expected that the mutual alignment shift may at worst be as large as 0.5 mrad ($=0.03^\circ$). However, even if an additional 0.1 mrad shift is taken into account, sufficient receiving power is expected for ranging at 25 km from the asteroid surface, based on the overlapping area between the fields of view of the transmitting and receiving telescopes.

Analysis of uncertainty in the LIDAR boresight direction

As described in section “Estimation of the LIDAR boresight”, the boresight of the receiving telescope was determined as the center of the circle with a diameter of 1.5 mrad that covers the directions at which signals from the ground were fully detected. Because there are other directions at which ground signals were detected outside

of this circle, the boresight we identified may still have an uncertainty of 1 mrad, i.e., the same amount as the step size of the scan. Here, we discuss the effects on range measurements near the asteroid if such uncertainty cannot be reduced. We first explain why the uncertainty does not affect ranging to the asteroid. Although there is no information about the alignment between the receiving and transmitting telescopes, we assume that the two telescopes overlap at least partially. This assumption is plausible based on the values of shifts in the vibration test and the thermal vacuum test described in 4.1. After arrival to the asteroid, the spacecraft will hover above the asteroid at a distance of about 20 km in what is called the home position. It will point the spacecraft's $-Z$ axis direction toward the asteroid to co-align instrument boresights for observation. At the home position, the distance between the LIDAR footprint and the sub-spacecraft point on the asteroid surface will be about 70 m, because the direction of the LIDAR boresight in the XY plane (referred to the spacecraft frame) is 3.5 mrad (0.2°). The footprint position may vary by up to 20 m if the uncertainty of the boresight direction is as high as 1 mrad. However, the diameter of the target asteroid, 162173 Ryugu, is about 900 m; therefore, it is unlikely that the LIDAR will lose its target if the spacecraft pointing is appropriate.

Next, we discuss the accuracy of the shape model of the asteroid if the uncertainty of the boresight persists in the case where no surface features, such as boulders, are found. As stated in section "Introduction", the estimated error in ranging to a position on the surface at a distance is D and a slope of α is $D(\Delta\theta) \sin \alpha$, if the installation error for the spacecraft structure is assumed to be $\Delta\theta$. If $\Delta\theta = 1$ mrad, $D = 20$ km, and $\alpha = 30^\circ$, the range error will be 10 m, which is equal to $10 \text{ (m)}/20 \text{ (km)} = 5 \times 10^{-4}$ in scaling the images taken with a visible camera. This ratio amounts to 0.45 m for the asteroid with a diameter of 900 m, or 0.15% volume error of the asteroid. This value is smaller than the scientific requirement of 5% discussed in section "Introduction". Therefore, the amount of uncertainty will not be a problem in scientific application, even if the current uncertainty cannot be reduced. However, when we try to estimate local topography using only LIDAR data, the errors of 20 m in determining footprint positions mentioned above may persist. Therefore, in this case, comparison with camera data, i.e., by finding prominent features like boulders or crater rims in the shape models, may be necessary.

As a related issue, the impact of albedo observation is evaluated. As explained in section "Experimental methods", the Hayabusa2 LIDAR is equipped with the energy monitor of the transmitted laser so that the ratio between the transmitted and received laser intensity can be used

to estimate the surface reflectance (albedo) of the asteroid. To estimate the albedo, we must determine what fraction of the transmitted laser is within the FOV of the receiving telescope. Unfortunately, because of the final design of the LIDAR, the beam divergence of the transmitted laser exceeds the FOV of the receiving telescope (Table 1); therefore, the alignment between the two telescopes is crucial. In the laser link experiment, no information was obtained because downlink signals were not detected, which may be a problem for estimation of the surface albedo.

Lastly, we consider possible confirmation of the alignment between the transmitting and receiving telescopes in orbit. Hayabusa2 drops five "target markers", which are 10-cm spheres covered with recursively reflective sheet, for touchdown onto the asteroid. The target markers can be used to estimate the common area of the transmitting and receiving fields of view. When a laser transmitted by LIDAR hits a target marker, the intensity of the return pulse will increase by a factor of 2 even from a 20 km altitude. The common area between the transmitting and receiving telescope fields of view can be constrained by detecting the enhancement of return pulses as a target marker moves into the field of view because of the rotation of the asteroid. It may also be possible to actively scan the spacecraft so that the laser can fire at target markers. The chances of such observations, however, are strongly dependent upon the direction of the rotation axis of the asteroid, as well as on the attitude control operation of the spacecraft. Because our a priori knowledge regarding those conditions is limited, quantitative discussion of these considerations is difficult before the spacecraft arrives at the asteroid.

Analysis of range mode received intensity observations

Significant changes in the received intensity by one order of magnitude were observed during the range mode testing from 16:15 to 16:30 on December 19. We suggest that these changes were caused by changes in atmospheric seeing and transparency, and therefore that these data do not reflect instrumental error. For example, during the lunar laser ranging (LLR), in which only a small number of photons can be detected, the return rate of the photons changes by two orders of magnitude even under the same lunar phase (Murphy et al. 2010). The situation is similar for SLR (Degnan 1993). Generally, the time scale of atmospheric fluctuations when atmospheric conditions are stable is expressed as the coherence time. Coherence time is given in milliseconds for infrared wavelengths of 1 μm ; therefore, the intensities observed in this time period may reflect different atmospheric conditions during 1-s sampling when the LIDAR was operating in range mode, and they are thus regarded as random. For

example, if we set the instantaneous atmospheric seeing as 3 arcsec, the received intensity may fall by 40% if the source intensity profile is assumed Gaussian, because the position of the intensity center moves 3 arcsec. In addition, atmospheric fluctuations will cause not only change in the position of the center but also change in the shape of the light source, which may contribute to the decrease in intensity as well.

Using the equation for the received intensity at the LIDAR given in section “[Laser link budget](#)”, if we set the distance as $D = 6.6$ million km and insert the other parameters of the ground station, the received intensity with the LIDAR can be calculated as

$$V = 3.17L_0(V).$$

If we set $L_0 = 0.5$ as the total efficiency due to loss, the equation yields 1585 mV, which is a comparable value to the maximum intensity of 1515 mV. Varying the value of efficiency by one order of magnitude may account for the one-order change in the received intensity.

At the same time, the received intensity at the LIDAR increased by more than one order of magnitude compared to the previous time period by setting an offset angle of 6 arcsec for the ground telescope. We do not have any good reason for the enhancement of the signal intensity because the time for the experiments was too limited to carry out further pointing tests. There are many unknown causes that may change the signal level, such as atmospheric fluctuations, and detailed discussion may not be useful. Therefore, we simply list some numbers related to pointing as follows. The position error of the spacecraft is estimated as <1 arcsec, and the pointing accuracy of the ground telescope is about 2 arcsec. In addition, the difference in transmitting and receiving aberrations, often described as point-ahead, was as small as 0.5 arcsec during the observation period. Therefore, telescope pointing at the nominal value must have been sufficient.

Status of the time transfer experiment

As stated in section “[Intervals between two received pulses](#)”, we could not associate the pulses from the ground station with the LIDAR pulses; therefore, the time transfer experiment (transfer of the ground time system to the spacecraft segment) was unsuccessful.

This difficulty arose because we were unable to establish two-way ranging. If two-way ranging could have been established, the arrival times of the ground pulses on the LIDAR could have been analyzed, because instrumental internal delay was obtained as telemetry data within the resolution of the LIDAR counter (1 count = 3.3 ns). With these data, time transfer may have been successful.

Lastly, resource limitations for the Hayabusa2 LIDAR during the instrument design phase precluded further

addition of hardware for precise time transfer. In the future, command reception timing and laser trigger timing should be synchronized to improve the accuracy in determining the absolute laser shot timing and spacecraft clock offset.

Summary

In this paper, we reported the results of a laser link experiment conducted using both the transponder mode and the range mode of the LIDAR aboard Hayabusa2. We carried out the experiments between the ground-based SLR stations and LIDAR when the spacecraft was near the Earth, before and after the gravity assist operation. The LIDAR detected the uplink laser pulses from the Mt. Stromlo station at a distance of 6.6 million km, and the boresight of the receiving telescope of the LIDAR was determined with an uncertainty of about 1 mrad. Hayabusa2 became the third spacecraft to establish a laser link with a ground station at a distance farther than the Moon, following the MESSENGER and Mars Global Surveyor missions. The following information was obtained from this experiment:

1. The boresight direction of the receiving telescope of the LIDAR was estimated with an uncertainty of about 1 mrad by scanning the spacecraft with a step of 1 mrad.
2. The received intensities with the LIDAR were estimated to be consistent with simple calculations assuming observation geometry, and the receiving system was confirmed to be sound.
3. As a time transfer experiment, pulse intervals sent from the ground station were retrieved from the LIDAR using telemetry data, and based on comparison of the histograms for the pulse intervals between the ground station and the LIDAR, we confirmed that the clock frequency of the LIDAR was adjusted successfully.

Furthermore, the following issues are open for further study:

1. A downlink signal from the LIDAR to the ground was not detected; therefore, two-way ranging was not established. As a result, alignment between the transmitting and receiving telescope could not be determined. At the target asteroid, the lack of this information should not be a problem as long as the ranging is successful. However, albedo estimation-based transmitted and received pulse intensities may be jeopardized because the fraction of the footprint that will be detected with the receiving telescope will be unknown. If there are many opportunities to

detect “target markers” by LIDAR, estimating the common area of the transmitting and receiving fields of view may be possible. However, the chances of observing the target markers may be limited because of the unknown direction of the rotation axis of the asteroid and spacecraft attitude control operation.

2. The accuracy assessment of the time transfer experiment was unsuccessful because the received pulses were not well time-tagged and the precise timing of reception was not obtained. Therefore, one-way ranging was not successful.

Although further studies are needed, these laser link experiments have proven to be an excellent method to confirm the performance of laser altimetry including the alignment measurement of the telescopes before spacecraft arrive at their target bodies. Checking performance before the arrival is important, especially for deep space missions, because travel to the destination takes a very long time and in-flight checking is not possible for laser altimeters.

Authors' contributions

HK, TM, HT, and YT participated in the design of the experiment since the early phase. HN, TM, NO, HT, TY, NN, TK, and TS contributed to data acquisition for the flight segment, including spacecraft orbit and attitude planning, and operation of the spacecraft and the instruments. HK, CM, and AP carried out the operation of the ground stations and data acquisition. HN and HS carried out data analysis. Finally, HN wrote the manuscript, and CM and AP revised the language. All authors read and approved the final manuscript.

Author details

¹ National Astronomical Observatory of Japan, Mitaka, Tokyo 181-8588, Japan.

² National Institute of Information and Communications Technology, Koganei, Tokyo 184-0015, Japan. ³ Institute of Space and Astronomical Science, Japan Aerospace Exploration Agency, Sagami, Kanagawa 252-0222, Japan.

⁴ Chiba Institute of Technology, Narashino, Chiba 275-0016, Japan. ⁵ Japan Aerospace Exploration Agency, Sagami, Kanagawa 252-0222, Japan.

⁶ Space Environment Research Centre, AITC2 Mt. Stromlo Observatory, Cotter Road, Weston Creek, ACT 2611, Australia. ⁷ NEC Corporation, Fuchu, Tokyo 183-8501, Japan.

Acknowledgements

We are grateful to the entire Hayabusa2 team. We thank Toshimichi Otsubo for discussion of prediction file contents and for operating the ground stations. During the experiment, Hayabusa2 was tracked by the NASA Deep Space Network Canberra station. We used the Generic Mapping Tool (GMT) software (Wessel and Smith 1991) for graph drawing. The authors thank Gregory A. Neumann and an anonymous reviewer for evaluating and improving this paper.

Competing interests

The authors declare that they have no competing interests.

Appendix 1: Observational modes of LIDAR

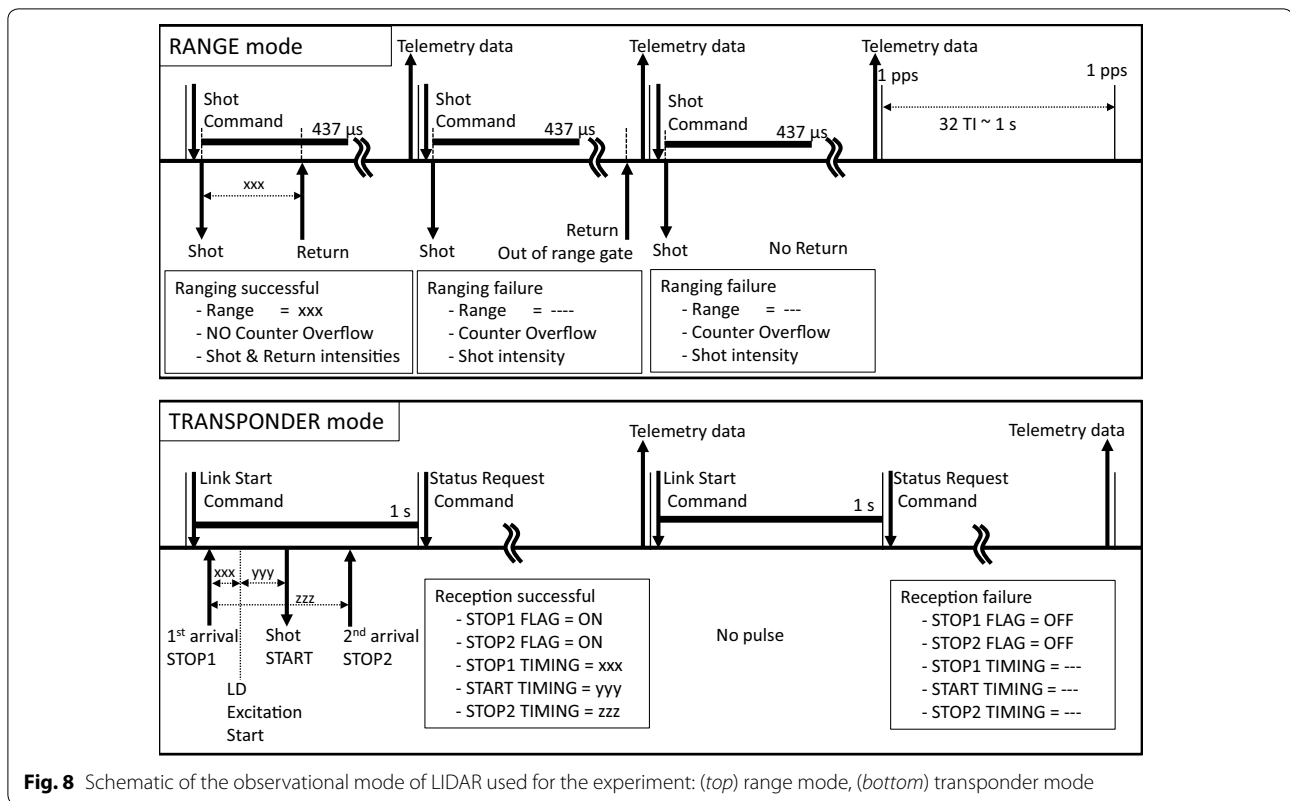
The following is an explanation of the range mode and transponder mode used for this experiment (Fig. 8). In range mode, continuous laser shot commands are issued at a maximum rate of once a second. After a shot command, a laser pulse of 15 mJ is emitted, and the detection range gate opens for 437 μ s. If a received pulse is detected

within this gate, the counter values of emission and reception are recorded, and these data are used for the calculation of the distance. At the same time, the intensities of the transmitted and received lasers are recorded. In cases when the return pulse is not received within the range gate or no return pulse is detected, the intensity of the sending laser and the status of counter overflow are recorded.

However, in the transponder mode, a link start command configures the instrument to wait for a maximum of 1 s for a laser pulse from the ground. If a signal over the threshold level is detected by the receiving telescope, the signal triggers laser emission of 15 mJ. Up to two laser pulses can be detected during the 1-s waiting period, and these pulses are flagged as the first and second pulse detection (the names of these telemetry data are STOP1 and STOP2). The interval between the first pulse and the laser diode trigger time (STOP1 TIMING), the interval between the laser diode trigger time to the laser emission (START TIMING), and the interval between two received pulses (STOP2 TIMING) are also recorded as telemetry data. If a laser pulse from the LIDAR can be detected on the ground, a two-way range is measured by subtracting the internal delay in the instrument, expressed as STOP1 TIMING + START TIMING. In the transponder mode, the intensities of the transmitting and receiving laser pulses are not available.

To retrieve data from the LIDAR in this mode, a status request command is issued. Therefore, if we require continuous data, these two commands must be issued every 2 s to acquire the data set. It has become clear that incorrect STOP pulses were being detected at the lower threshold because of noise thought to originate from the analog–digital converter. Note that a lower threshold value compared to the value used for normal ranging near the asteroid was set so that faint laser pulses could be detected during the spacecraft scan in this experiment.

The LIDAR has a 17-bit counter with about 300 MHz (3.3 ns/bit), a single cycle of which is about 437 μ s. More precisely, the value of 299,788,710.6 Hz is used for the counter at room temperature. The pulse intervals from the ground stations are 0.1 s (10 Hz) for the NICT Koganei station and 5.882 ms (170 Hz) for the Mt. Stromlo station; therefore, the raw counter values of the pulse interval (STOP2 TIMING) must be corrected by taking into account the cycle ambiguities to retrieve the exact counter values corresponding to the length of the pulse interval. For example, the cycle ambiguity for the 170 Hz pulse repetition of the Mt. Stromlo station is 13, and the remainder of the counter (\sim 59,500) divided by 2^{17} ($=$ 131,072) is obtained as the raw telemetry data. In addition, two successive pulses are not necessarily detected if



the received laser power is low; therefore, we must estimate how many gaps are included in the observed counter value for STOP2.

Appendix 2: Explanation of sparse data in the range mode

Sparse data in the range mode in section “Intensity of received pulses in range mode” can be explained by slight differences between the Time Index (TI) and UTC, as well as the motion of the spacecraft. In this mode, only pulses received within 437 μ s after the 1 pps (i.e. laser shot) can be detected, which corresponds to one-cycle length of the counter (Fig. 9). The laser shot of the LIDAR is based on the 1 pps derived from 32 TIs, not to exactly 1 UTC second, whereas shots from the ground-based telescope are based on the UTC time interval. This discrepancy generates an apparent delay in the range counter for the arrival time of the shots from the ground because at that time, 32 TIs is slightly shorter than 1 UTC second. According to the TI–UTC relation table, the exact value of 1 TI was 31.2495665 ms. The apparent “shift velocity” in the range gate was calculated to be:

$$1.0 - 32 \times 0.0312495665 \text{ (s)} = 13.87008 \text{ (}\mu\text{s)}.$$

This result indicates that a pulse emitted 1 UTC second after a particular pulse arrives 13.87 μ s later at the position in the counter. Similarly, the spacecraft motion, which has positive velocity away from the Earth, causes a positive shift in the counter. At the time of the experiment, the line-of-sight velocity was approximately $v = 4.42 \text{ (km/s)}$, which allowed the “shift velocity” in the counter associated with the spacecraft motion to be calculated, given the speed of light, $c = 299,792,458 \text{ (m/s)}$, as

$$4420 \text{ (m/s)} / c \text{ (m/s)} = 14.743533 \text{ (}\mu\text{s/s)}.$$

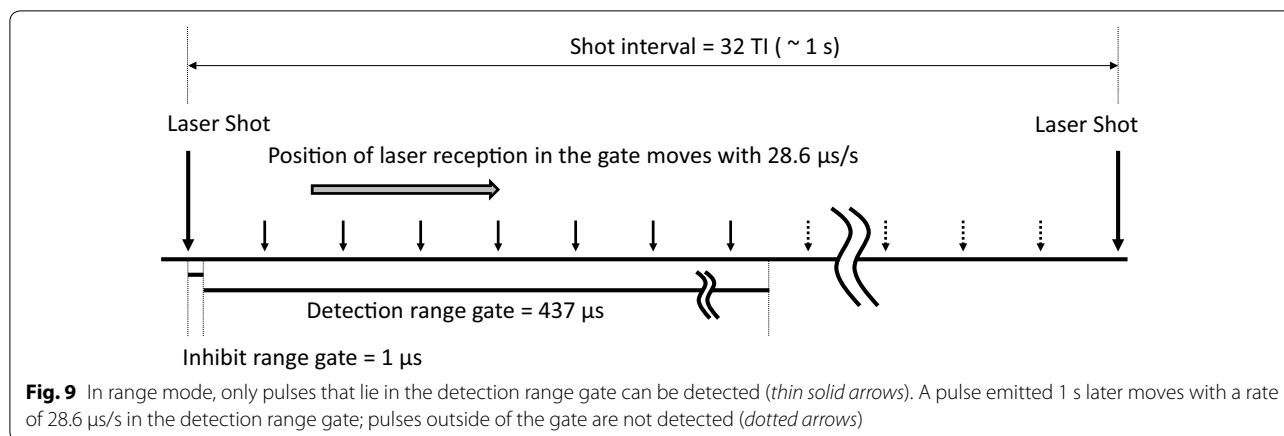
The total “shift velocity” in the range gate was then calculated to be $13.870 + 14.743 = 28.613 \text{ }\mu\text{s/s}$. Therefore, the length of the range gate divided by $28.613 \text{ }\mu\text{s/s}$, or

$$437 \text{ (}\mu\text{s)} / 28.613 \text{ (}\mu\text{s/s)} = 15 \text{ (s)}$$

gives the total number of the data points in one slot. The length of time between two ground pulses divided by this “shift velocity”,

$$5882.35 \text{ (}\mu\text{s)} / 28.613 \text{ (}\mu\text{s/s)} = 205.58 \text{ (s)},$$

gives the time interval between data slots. Actually, the time interval was 203 s (=3 min and 23 s), which confirms the above calculation.



Received: 22 June 2016 Accepted: 13 December 2016
Published online: 03 January 2017

References

- Abe S, Mukai T, Hirata N, Barnouin-Jha OS, Cheng AF, Demura H, Gaskell RW, Hashimoto T, Hiraoka K, Honda T, Kubota T, Matsuoka M, Mizuno T, Nakamura R, Scheeres DJ, Yoshikawa M (2006) Mass and local topography measurements of Itokawa by Hayabusa. *Science* 312:1344–1347
- Abshire JB, Sun X, Neumann G, McGarry J, Zagwodzki T, Jester P, Riris H, Zuber M, Smith DE (2006) Laser pulses from Earth detected at Mars. In: Proceedings of the conference on lasers and electro-optics (CLEO)
- Degnan JJ (1993) Millimeter accuracy satellite laser ranging: a review. In: Smith DE, Turcotte DL (eds) *Contributions of Space Geodynamics: Technology*. AGU Geodynamics Series 25:133–162
- Fridelance P, Veillet C (1995) Operation and data analysis in the LASSO experiment. *Metrologia* 32:27–33
- Fridelance P, Samain E, Veillet C (1997) T2L2-time transfer by laser link: a new optical time transfer generation. *Exp Astron* 7:191–207
- Mizuno T, Tsuno K, Okumura E, Nakayama M (2006) LIDAR for asteroid explorer Hayabusa: development and on board evaluation. *JJSASS* 54(634):514–521
- Mizuno T, Kase T, Shiina T, Mita M, Namiki N, Senshu H, Yamada R, Noda H, Kunimori H, Hirata N, Terui F, Mimasu Y (2016) Development of the laser altimeter (LIDAR) for Hayabusa 2. *Space Sci Rev*. doi:10.1007/s11214-015-0231-2
- Murphy TW Jr, Adelberger EG, Battat JBR, Hoyle CD, McMillan RJ, Michelsen EL, Samad RL, Stubbs CW, Swanson HE (2010) Long-term degradation of optical devices on the Moon. *Icarus* 208:31–35
- Namiki N, Mizuno T, Hirata N, Noda H, Senshu H, Yamada R, Ikeda H, Abe S, Matsumoto K, Oshigami S, Shizugami M, Yoshida F, Hirata N, Miyamoto H, Sasaki S, Araki H, Tazawa S, Ishihara Y, Kobayashi M, Wada K, Demura H, Kimura J, Hayakawa H, Kobayashi N (2014) Scientific use of LIDAR data of Hayabusa-2 mission. In: Ip WH (ed.) *Proceedings of CJMT-1*, pp 74–98
- Prochazka I, Schreiber U, Schaefer W (2011) Laser time transfer and its application in the Galileo programme. *Adv Space Res* 47:239–246
- Samain E, Exertier P, Guillemot Ph, Pierron F, Albanese D, Paris J, Torre JM, Leon S (2010) Time transfer by laser link-T2L2: current status of the validation program. In: *Proceedings of EFTF-2010 24th European frequency and time forum*, pp 1–8. doi:10.1109/EFTF.2010.6533652
- Senshu H, Oshigami S, Kobayashi M, Yamada R, Namiki N, Noda H, Ishihara Y, Mizuno T (2016) Dust detection mode of the Hayabusa2 LIDAR. *Space Sci Rev*. doi:10.1007/s11214-016-0242-7
- Smith D, Zuber MT, Sun X, Neumann GA, Cavanaugh JF, McGarry JF, Zagwodzki TW (2006) Two-way laser link over interplanetary distance. *Science* 311:53
- Smith C, Gao Y, Sang J, Greene B (2012) Laser tracking of space debris for precision orbit determination. *Proc AAS/AIAA Astrodyn Spec Conf Adv Astronaut Sci* 142(11–417):1–10
- Wessel P, Smith WHF (1991) Free software helps map and display data. *EOS Trans AGU* 72:441
- Yamada R, Senshu H, Namiki N, Mizuno T, Abe S, Yoshida F, Noda H, Hirata N, Oshigami S, Araki H, Ishihara Y, Matsumoto K (2016) Albedo observation by Hayabusa 2 LIDAR: instrument performance and error evaluation. *Space Sci Rev*. doi:10.1007/s11214-016-0240-9
- Yang F, Peicheng H, Zhongping Z, Wanzhen C, Haifeng Z, Yuanming W, Wendong M, Jie W, Guangnan Z, Ying L, Luyuan W, Prochazka I, You Z, Cunbo F, Xingwei H (2008) Preliminary results of the laser time transfer (LTT) project. In: *Proceedings of the 16th international workshop on laser ranging*, pp 690–694
- Sun X, Barker MK, Mao D, Mazarico E, Neumann GA, Skillman DR, Zagwodzki TW, Torrence MH, McGarry J, Smith DE, Zuber MT (2014) In-orbit calibration of the lunar orbiter laser altimeter via two-way laser ranging with an Earth station. *American Geophysical Union, Fall Meeting 2014*, abstract #P13B-3814

Submit your manuscript to a SpringerOpen® journal and benefit from:

- Convenient online submission
- Rigorous peer review
- Immediate publication on acceptance
- Open access: articles freely available online
- High visibility within the field
- Retaining the copyright to your article

Submit your next manuscript at ► springeropen.com